J Mar Sci Technol (1996) 1: 114–124

Journal of
Marine Science
and Technology

Nonlinear hydroelastic behavior of propellers using a finite-element method and lifting surface theory

HUEI-JENG LIN and JIUNN-JYI LIN

Department of Naval Architecture and Ocean Engineering, National Taiwan University, 73 Chow-Shan Road, Taipei, Taiwan

Abstract: A finite-element method coupled with analysis of a noncavitating lifting surface was used to assess the performance of a marine propeller, including the thrust, torque, efficiency coefficients, and deflections. The formulation used displacements as unknowns in the structural part and the strength of the vortex as unknowns in the fluid part. A coupled matrix derived from the Bernoulli equation and hydrostatic pressure in terms of the strength of the vortex enforced coupling between the fluid and the structure. The resulting matrix equation was unsymmetric and nonlinear; a Newton-Raphson procedure was used to solve this equation. The numerical results were compared with test data; computed and measured values agreed satisfactorily. We also investigated the effect of blade thickness on the performance and strength of the propeller. We did not consider the fatigue strengh of the propeller in this analysis.

Key words: hydroelastic, geometrical nonlinear, lifting surface, coupled fluid–structure iteration

List of symbols

a	length of plate
b	width of plate or beam
C	chord length of propeller section
D	diameter of propeller
E	young's modulus
h	thickness of plate or beam
I	section modulus of beam
J	advance coefficient (V_a/nD)
K_T	thrust coefficient ($T/\rho n^2 D^4$)
K_Q	torque coefficient ($Q/\rho n^2 D^5$)
L	length of beam
n	rotational speed of propeller
P	pitch of propeller
r	radial coordinate
R	radius of propeller
$1/R_Y$	curvature of plate
q	density of distribution load
Q	torque moment of propeller
T	thrust force of propeller
u_1	displacement along X axis
u_2	displacement along Y axis
u_3	displacement along Z axis
V_a	advance speed of ship
W	central deflection of plate or tip deflection of beam
Ω	rotation speed, $\Omega = \{\Omega_x, \Omega_y, \Omega_z\}$
θ	angle of attack (between 0° and 90°)
ω_0	fundamental natural frequency
η_0	efficiency ($TV_a/2n\pi Q$)
ρ	density of flow

Address correspondence to: H.-J. Lin
Received for publication on June 7, 1995; accepted on Nov. 13, 1995

Introduction

The hydrodynamic aspects of the design of marine propellers must be considered to the deflection and strength of the propeller blade and to maximize its efficiency. A procedure to calculate the blade strength must involve numerical methods because of the nonlinear phenomena of blade deflection and loading. A geometrically nonlinear calculation is needed to calculate the quasistatic deflection of the blade that results from the centrifugal force and the distribution of pressure in the fluid.

The first approach to analyze the strength of the blade was proposed by Taylor,[1] who considered a propeller blade to be a cantilever rigidly attached to a boss. The stresses were calculated using elementary beam theory for cylindrical blade sections having a straight face and a curved back. The cantilever beam theory yields reasonable estimates of stresses at certain selected points of relatively straight, narrow blades. Modified forms of this theory were proposed for a wide propeller blade, but the results for the structural response of the blade were limited.

The shell theory approach was first proposed by Cohen,[2] who considered a propeller blade to be a helicoid shell of variable thickness and infinite width. This approach was of limited use when applied to a blade of finite width. Conolly[3] developed a thin-shell approach in parallel with an experimental program. This approach was demonstrated to be successful for a wide blade, but the assumption of symmetrical forms and invariant normal deflection of a section limited the application of the method. Moreover shell-type theories that incorporate broad assumptions are used for routine design work.

The reason for choosing the finite-element method for the current study is its lack of any additional assumptions about the behavior of the displacements. As with the shell theory, several assumptions are made in the formulation of finite-element theory. When we use a finite-element procedure to predict the deflection and strength of the blade, we need the blade geometry and loading data as input to the procedure. The geometry of the blade is generally obtained using the radial distribution of skew, rake, pitch, and two-dimensional wing profile data; these quantities are fitted with a surface-fitting or cubic-spline-fitting routine. The pressure acting normally on the surface of the blade is calculated at the fluid analysis grid points according to various methods, including two-dimensional wing theory, lifting line, lifting surface, and the panel method and is interpolated at structural grid points.

Genalis[4] used a triangular plane element and Atkinson[5] used a parabolic and curved element of a thick shell model to analyze a mathematically defined propeller. These results were compared with calculated and experimental results presented by Conolly.[3] It was concluded that the thick-shell model is satisfactory to calculate the response of a propeller blade. Ma[6] applied the isoparametric solid-element model to analyze a highly skewed propeller; the computed results were compared with measured deflections and stresses under a steady pressure. Sontvedt[7] applied a triangular thin-shell element to analyze moderately skewed and highly skewed propellers under constant hydrodynamic loading. The calculated results of stresses and deflection were compared with experiments. Atkinson and Glover[8] applied a curved superparametric thick-shell element model to analyze three types of propellers. The surface loading was calculated according to an unsteady lifting surface analysis developed by Szantyr.[9] In this process, the surface pressure was first obtained by assuming that the structure is rigid and the resulting surface pressure is imposed on the structure to calculate the structural response. An iterative procedure was applied to calculate a new blade geometry and to modify the surface loading. The process was repeated until a new stable condition was achieved; this approach was applied in an uncoupled manner.

In the current study, a coupled fluid–structure analysis procedure was developed for calculating the performance and strength of the propeller. The calculation used a geometrically nonlinear finite-element procedure for the structural analysis and the non-cavitating lifting surface theory for the fluid analysis. It applied the steady Bernoulli equation to calculate the pressure difference at structural mesh points and established a coupled matrix of interaction between fluid and structure. We combined these matrices including a structural stiffness matrix and an influence matrix for the fluid, and analyzed the coupled matrix resulting in an a unsymmetric and nonlinear governing equation. Then we applied a Newton-Raphson procedure to solve this equation. The results of the calculation show that the deflection of the blade alters the distribution of the blade pitch and camber and affects the performance of the propeller. We also shown how the blade thickness affects the strength and performance of the propeller. The strength of the blade was justified according to the Tresca yield criterion. We did not consider the fatigue strength of the propeller, although it is important in propeller design.

Finite-element formulation

Because of the nature of blade geometry and loading, structural analysis of the propeller is possible only by means of numerical methods. The main advantage of finite-element modeling is its general applicability to a complicated blade geometry. The blade of the propeller is described as a shallow shell and is modeled with a

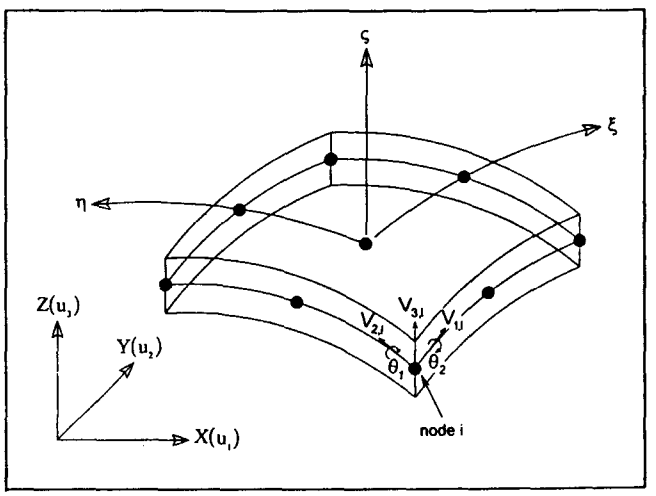

Fig. 1. Typical three-dimensional degenerate nine-node shell element

three-dimensional degenerate nine-node shell element. A geometrically nonlinear calculation is applied to calculate the deformation of the propeller blade and its quasistatic deformation resulting from centrifugal and hydrostatic forces.

Three-dimensional degenerate nine-node shell element

In the present work, a geometrically nonlinear nine-node degenerate shell element[10] (Fig. 1) is applied. The coordinates of a typical point in the element can be interpolated according to

$$X_i = \sum_{j=1}^{9} N_j(\xi, \eta) \cdot \left[x_i^j + \frac{1}{2}\varsigma \cdot t_j \cdot v_{3,i}^j \right] \quad i = 1,2,3 \tag{1}$$

and the displacement according to

$$u_i = \sum_{j=1}^{9} N_j(\xi, \eta) \cdot \left[u_i^j + \frac{1}{2}\varsigma_j \cdot t_j \cdot (\theta_1^j v_{1,i}^j - \theta_2^j v_{2,i}^j) \right]$$

$$i = 1,2,3 \tag{2}$$

In Eqs. 1, 2, (ξ, η, ζ) are the natural coordinates that lie between -1 and 1, $N_j(\xi, \eta)$ is the Lagrange family of interpolation function of a two-dimensional element, t_j is the thinkness at node j, and $v_{3,i}^j$ are components of the unit vector normal to the shell midsurface at note j. $v_{1,i}^j$ and $v_{2,i}^j$ are two orthogonal vectors normal to $v_{3,i}^j$, with corresponding rotations θ_2^j and θ_1^j. At each node there are five degrees of freedom, i.e., u_1, u_2, u_3, θ_1, θ_2. The finite-element equation for a geometrically nonlinear three-dimensional degenerate shell element is written as

$$([K_0] + [K_L] + [K_G])\{u\} = \{F_{ext}\} + \{F_I\} \tag{3}$$

in which $[K_0]$, $[K_L]$ and $[K_G]$ are the linear stiffness matrix, initial displacement matrix, and geometric matrix, $\{u\}$ is the nodal displacement, $\{F_{ext}\}$ are the external forces excluding fluid forces $\{F_I\}$. The matrices are defined as[10]

$$[K_0] = \int_{\text{vol}} B_0^T D B_0 d\text{Vol}$$

$$[K_L] = \int_{\text{vol}} (B_0^T D B_L + B_L^T D B_L + B_L^T D B_0) d\text{Vol}$$

$$[K_G] = \int_{\text{vol}} \mathrm{G}^{\mathrm{T}} \begin{bmatrix} \sigma_x & \tau_{xy} \\ \tau_{xy} & \sigma_y \end{bmatrix} G \cdot d\text{Vol} \tag{4}$$

In these equations, B_0 and B_L are linear and nonlinear strain–displacement transformation matrices, D is the material property matrix, and G is a matrix defined purely in terms of coordinates. The equation is formed on the basis of an updated Lagrangian description[11] and is solved according to the Newton-Raphson procedure.[12] The first sample[13] is that a cantilever beam subjected to a uniformly distributed follower load was calculated. The second and third samples[14] are a square plate supported by a simple support and clamped edge respectively, subjected to a uniform pressure. Figures 2 and 3 show the results of numerical calculations and analytic solutions. It is shown that the numerical and analytic solutions agree satisfactorily.

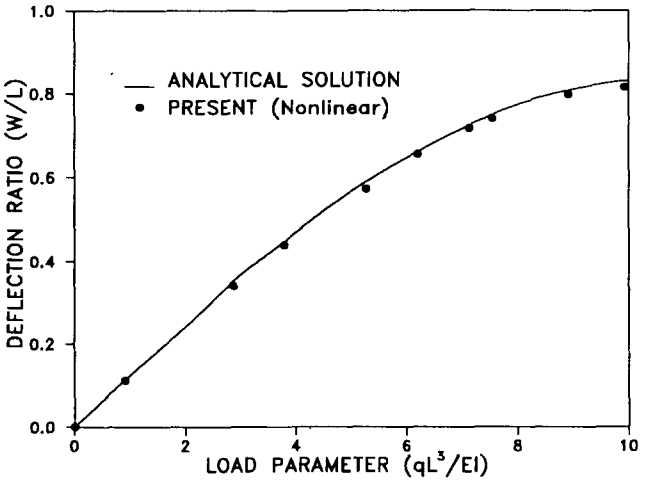

Fig. 2. Large deflection analysis of a cantilever under a uniformly distribute load

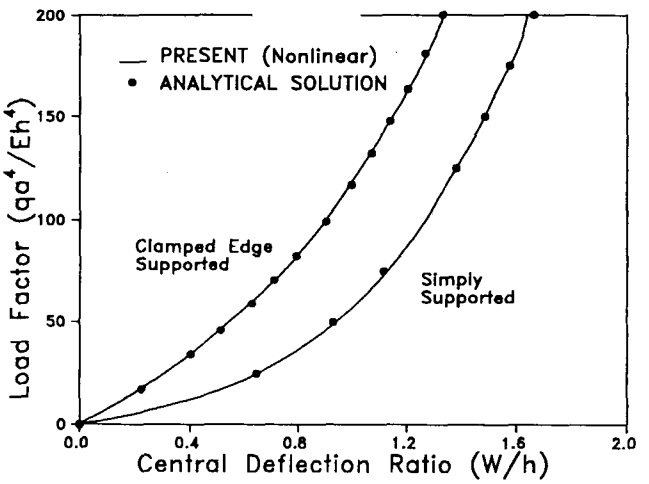

Fig. 3. Large deflection analysis of a plate subjected to uniform pressure

Rotational stiffness matrix and centrifugal load

The calculation of the rotating propeller includes rotational effects, i.e., the rotational stiffness matrix and the centrifugal load. We derive these by applying the Lagrange equation and the kinetic energy of the propeller blade.[15] The expression for the rotational stiffness matrix is

Table 1. Effect of rotational speed and angle of attack on natural frequencies

Rotation ratio	Angle of attack (deg)	Mode	Symmetric		anti-symmetric	
			Ref. 15	Present	Ref. 15	Present
0	all	1	138.5	140.0	86.0	86.2
		2	250.0	250.8	345.0	345.7
		3	392.3	390.1	578.5	546.5
		4	736.7	744.6	742.2	770.4
1	0	1	170.3	170.5	151.0	153.8
		2	301.9	281.2	418.2	407.8
		3	463.5	469.8	623.4	596.4
		4	789.1	657.8	829.0	794.1
1	45	1	150.2	159.5	110.2	128.3
		2	266.6	266.8	404.9	402.9
		3	448.1	455.3	592.4	577.8
		4	780.6	706.9	819.6	803.5
1	90	1	147.8	140.6	105.1	89.9
		2	262.7	255.3	403.5	400.2
		3	446.5	442.3	589.1	556.6
		4	779.8	781.3	818.6	817.2

These data are for a steel blade, length of 30 cm ($a/b = 1$, $a/R_y = 0.5$, $a/h = 100$). All data are in H_z. Rotation ratio, Ω/ω_0; symmetric, bending mode; anti-symmetric, torsion mode

$$[K_R] = \rho \int_{vol} [N_s]^T [A][N_s] \cdot d\text{Vol}$$

$$[A] = \begin{bmatrix} \Omega_y^2 + \Omega_z^2 & -\Omega_x\Omega_y & -\Omega_x\Omega_z \\ -\Omega_x\Omega_y & \Omega_x^2 + \Omega_z^2 & -\Omega_z\Omega_y \\ -\Omega_x\Omega_z & -\Omega_z\Omega_y & \Omega_x^2 + \Omega_y^2 \end{bmatrix} \tag{5}$$

In Eq. 5, $[N_s]$ is the displacement interpolation matrix, $[A]$ is the angular velocity matrix, and ρ is the density of the blade. The expression of the centrifugal load is

$$\{F_R\} = \rho \int_{\text{vol}} [N_s]^T [A] \begin{Bmatrix} x \\ y \\ z \end{Bmatrix} \cdot d\text{Vol} \tag{6}$$

Then the finite-element equation for the propeller blade subjected to a centrifugal force is obtained by combining Eqs. 3, 5, and 6

$$([K_0] + [K_L] + [K_G] - [K_R])\{u\} = \{F_{ext}\} + \{F_I\} + \{F_R\} \tag{7}$$

The verified sample[16] is that a cambered blade clamped at one side rotates at the fundamental natural frequency (ω_0). The effect of varying the angle of attack (θ) is demonstrated in Table 1. It is seen that the results of Sreenivasamurthy and Ramamurti[15] and the current study agree well, the use of Eq. 7 is valid to calculate the structural response in this analysis.

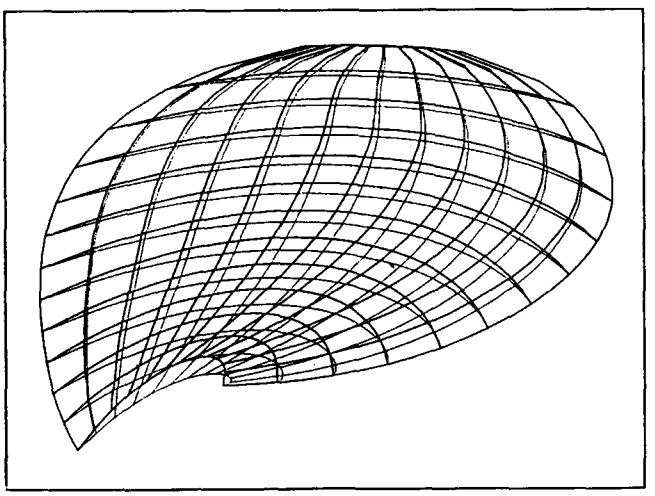

Fig. 4. Generation of a propeller mesh

Generation of a finite-element mesh

The finite-element mesh used is that which Kerwin and Lee[17] used for their lifting surface calculation. This mesh describes only the camber surface of the blade. We include the thickness in our calculation and use this grid for both sides of the blade. Thus, the coordinates of a point on the face or back surface of the key blade can be written as

$$X = r\cos\theta$$

$$Y = r\sin\theta$$

$$Z = Z_m + c\left(s - \frac{1}{2}\right)\sin\varphi - \left(f \pm \frac{t}{2}\right)\cos\varphi$$

$$\theta = \theta_m + c\left(s - \frac{1}{2}\right)\frac{\cos\varphi}{r} + \left(f \pm \frac{t}{2}\right)\frac{\sin\varphi}{r} \tag{8}$$

In Eq. 8, X, Y and Z are the spatial coordinates of the blade and describe the face and back of blade. They are expressed by the radial variation of skew $\theta_m(r)$, rake $Z_m(r)$, pitch angle $\varphi(r)$, and chord-length $c(r)$ and the chord-variation of camber $f(s)$, and thickness $t(s)$ in terms of chordwise coordinate s. These geometrical quantities are all represented by cubic spline functions of suitably stretched coordinates, based on values specified or computed at a set of radial and chordwise stations. Figure 4 shows the result of a finite-element mesh for a MAU 3-60 propeller blade.

Lifting surface theory

The steady and noncavitating lifting surface analysis procedure used in the current study is that of Kerwin and Lee.[17] The blades are assumed sufficiently thin that their presence in the unbounded fluid can be represented by the distribution of vortices and sources lying on the mean camber surface of each blade, together with a distribution of trailing vortices into the wake. The generation of the mean camber surface of the blade is defined by means of the radial variation of skew, rake, pitch, and chordwise variation of camber.

The method employs a discrete vortex/source lattice of concentrated straight-line elements to represent a continuous singularity distribution with elements located on the exact camber surface of the blade and with velocities computed at a prescribed number of control points properly located in relation to the lattice. The vortex/source singularities are distributed on trial surfaces representing the blades and their trailing vortex wake; the velocities induced by these singularities are computed and the trial surfaces are then realigned with the resultant flow. The process is repeated until the wake parameters or circulation converge. The presence of the ship hull, propeller hub, and free surface is ignored and the flow is considered as inviscid. The viscous effects arise in the traditional manner of estimating blade frictional drag and are determined on introducing a drag coefficient C_D.

The strength of a vortex or source is determined from the solid boundary condition at the control point of each lattice element, expressed as

$$\vec{n} \cdot \vec{V}_{T,i} = 0 \quad i = 1,2,\ldots,(N \times M) \tag{9}$$

In Eq. 9, $\vec{n}_i$ represents the normal vector of control point i, $\vec{V}_{T,i}$ is the total velocity of control point i, which includes the inflow velocity $\vec{V}_\infty$, propeller rotational velocity $\vec{V}_\Omega$, and velocity $\vec{V}_q$ induced by vortex or source singularities. The strength of the sources representing the blade thickness is predetermined by a stripwise application of thin-wing theory at each radius, leaving only the vortex strengths to be determined. Thus the vortex system is organized into horseshoe vortices. Each horseshoe vortex consists of a spanwise vortex and two trailing vortices extending along the blade and along the trailing wake. The horseshoe vortex strengths on other blades can be expressed in terms of those on the key blade. Equation 9 becomes converted into simultaneous equations to determine the key blade horseshoe vortex strengths Γ. The formulations are expressed as

$$\sum_{j=1}^{(N\times M)} A_{ij}\Gamma_i + \vec{n}_i \cdot (\vec{V}_\infty + \vec{V}_\Omega + \vec{V}_q^{\text{source}})_i = 0$$

$$i = 1,2,\ldots,N \times M \tag{10}$$

In Eq. 10, A_{ij} is defined as an influence coefficient which is the normal velocity at control point i caused by a unit strength horseshoe vortex j. The total number of unknowns (Γ) equals the number of control points ($N \times M$) on the key blade. The matrix form of above equation is expressed as

$$G\Gamma = -\vec{n} \cdot (\vec{V}_\infty + \vec{V}_\Omega + \vec{V}_q^{\text{source}}) \tag{11}$$

In this study, the usage of the program is mainly to calculate the total velocities $\vec{V}_T$ at structural mesh points in conjunction with the Bernoulli equation to calculate the coupled matrix for the fluid and structure, described in the next section.

Fluid–Structure interaction

We employed, the steady Bernoulli equation to calculate the pressure on the face and back of the blade at the structural element mesh points. Thus we evaluate the pressure difference ΔP of structural mesh points to calculate the coupled matrix of interaction between fluid and structure.

Aplication of the bernoulli equation

The pressure of a point in an unbound fluid is calculated according to the Bernoulli equation, if the flow is in a steady condition. It is expressed as

$$P - P_\infty = \frac{1}{2}\rho(V_\infty^2 - V^2) \tag{12}$$

In Eq. 12, $V^2 = \vec{V} \cdot \vec{V}$ and $\vec{V} = \vec{V}_\infty + \vec{V}_\Omega + \vec{V}_q$ and ρ is the density of the fluid. Equation 12 becomes

$$P - P_\infty = -\frac{1}{2}\rho\left[2\vec{V}_\infty \cdot \vec{V}_\Omega + V_\Omega^2 + 2\left(\vec{V}_\infty + \vec{V}_\Omega + \frac{1}{2}\vec{V}_q\right)\right] \cdot \vec{V}_q \tag{13}$$

In which, $\vec{V}_q \cdot \vec{V}_q$ is a quadratic term for which we use $\vec{V}_{q,i-1} \cdot \vec{V}_{q,i}$ for linearization; the subscript i and $i-1$ denote the iteration number. The pressure difference between the face and back of the blade is expressed as

$$\Delta P = (P - P_\infty)_{\text{face}} - (P - P_\infty)_{\text{back}} \tag{14}$$

Substituting Eq. 13 into Eq. 14, we obtain

$$\Delta P = \rho\left[\left(\vec{V}_\infty + \vec{V}_\Omega + \frac{1}{2}\vec{V}_{q,i-1}\right) \cdot \vec{V}_{q,i}|_{\text{back}} - \left(\vec{V}_\infty + \vec{V}_\Omega + \frac{1}{2}\vec{V}_{q,i-1}\right) \cdot \vec{V}_{q,i}|_{\text{face}}\right] \tag{15}$$

In Eq. 15, $\vec{V}_q{}^i$ is the velocity induced by vortex and source singularities at iteration i and is the only term to be evaluated. It is expressed as

$$\vec{V}_q = \sum_m \sum_n u_{mn}^{\text{vortex}} \Gamma_{mn}^{\text{vortex}} + \sum_m \sum_n u_{mn}^{\text{source}} \Gamma_{mn}^{\text{source}} \tag{16}$$

In Eq. 16, u_{mn} is the velocity induced by a unit strength vortex or source calculated according to the Biot-Savart law. The strength of sources Γ^{source} is previously determined with a stripwise application of thin-wing theory at each radius, leaving only vortex strengths Γ^{vortex} to be determined. Equation 15 becomes

$$\Delta P = \rho \sum_m \sum_n \left[\left(\vec{V}_\infty + \vec{V}_\Omega + \frac{\vec{V}_{q,i-1}}{2}\right) \cdot u_{mn}^{\text{vortex}}|_{\text{back}} - \left(\vec{V}_\infty + \vec{V}_\Omega + \frac{\vec{V}_{q,i-1}}{2}\right) \cdot u_{mn}^{\text{vortex}}|_{\text{face}}\right] \cdot \Gamma_{mn}^{\text{vortex}} + \text{SOURCE} \tag{17}$$

in which *SOURCE* is the pressure difference calculated from the source singularity, which can be neglected if we ignore the effect of the blade thickness. In matrix form, the pressure difference ΔP is expressed as

$$\Delta P = \{AC\}^T\{\Gamma^{\text{vortex}}\} + \text{SOURCE} \tag{18}$$

The coupled fluid—structure matrix

The forces of the fluid acting on the blades are expressed as[18]

$$F_I = \int_A N_s^T n \cdot P dA \tag{19}$$

in which dA is the interaction boundary between fluid and structure and n is its outward normal vector. P is the pressure o fluid acting on the structure, defined as

$$P = [N]\{\Delta P\} \tag{20}$$

in which $[N]$ is the interpolation matrix consisting of the Lagrange family of interpolation functions and $\{\Delta P\}$ is the matrix of pressure difference calculated according to Eq. 18. Equation 19 becomes

$$\begin{aligned} F_I &= \int_A N_s^T n N dA \cdot \{\Delta P\} \\ &= [A]\{\Delta P\} \\ &= [A] \cdot ([AC]^T\{\Gamma^{\text{vortex}}\} + \{\text{SOURCE}\}) \\ &= [B]\{\Gamma^{\text{vortex}}\} + \{C\} \end{aligned} \tag{21}$$

in which, $[B]$ is the coupled matrix of interaction between fluid and structure, $[C]$ is the matrix determined from the distribution of the blade thickness, which can be neglected if the thickness effect of the blades is ignored.

The finite-element Eq. 6 coupled with Eq. 21 is modified to

$$([K_0] + [K_L] + [K_G] - [K_R])\{u\} - [B]\{\Gamma\} = \{F_{ext}\} + \{F_R\} + \{c\} \tag{22}$$

Substituting Eq. 11 into Eq. 22, we obtain

$$\begin{bmatrix} K_T(u) & -B(u) \\ 0 & G(u) \end{bmatrix} \begin{Bmatrix} u \\ \Gamma \end{Bmatrix} = \begin{Bmatrix} F_R(u) + F_{ext} + C \\ RHS(u) \end{Bmatrix} \tag{23}$$

in which, matrices K_T, B, G, F_R, and RHS are functions of displacement variables u. Thus a nonlinear procedure must be applied to solve Eq. 23. The blades are subjected to viscous drag forces as well as the pressure force. The drag force is assumed to act in the chordwise direction and is expressed as

$$F_D = \frac{1}{2} \cdot C_D \cdot \rho \cdot A_{element} \cdot V_T^2 \tag{24}$$

in which C_D is the drag coefficient determined experimentally, $A_{element}$ is the area of the structural element, and V_T^2 is the squared value of the total velocity at the center of the structural element. The procedure used to derive the coupling matrix is also used to derive the added coupling matrix resulting from the F_D force and adds the latter matrix to matrix B of Eq. 23. We used the Newton-Raphson procedure to solve Eq. 23, and we adopted three convergence criteria in the structural calculation (the displacement of the blade, the external forces, and the external work) and two convergence criteria in the fluid calculation (the wake velocities just behind the trailing edge and the strength of the singularity) for every iteration.

Numerical example and discussion

The approach discussed above was applied to calculate the performance of a MAU 3-60 model propeller to verify the program. The MAU 3-60 model propeller

has three blades, expanded area ratio of 0.6, a diameter of 20 cm, and is made of bronze. This propeller was subjected to experiments in the laboratory of the National Taiwan University. Computation was performed on an HP 9000 computer. We calculated the performance of the MAU 3-60 propeller to test the validity of the program; the numerical results are compared with those from experiments. We also constructed a linear approach for comparison with the nonlinear approach. The linear approach is an uncoupled procedure. The structural stiffness K_T of the linear approach is presented as linear stiffness matrix $[K_0]$ and rotational stiffness $[K_R]$. The influence matrices B, G, and RHS are not functions of displacement variables u. The procedure for the linear approach assumes the structure to be rigid when the fluid response is calculated. Then the resulting pressure is imposed on the structure to obtain the structural response. The calculation is repeated between fluid and structure until convergent conditions are satisfied. The convergent criteria of the linear approach account for the displacement of the blade, wake velocities, and the strength of singularities and does not consider the equilibrium condition between external and internal forces. We evaluated the strength of the propeller for effects of blade thickness because the existing methods produce propellers that are excessively strong, i.e., failures are comparatively rare. We decreased the blade thickness to calculate the strength of the blade according to the Tresca yield criteria in an effort to learn how a decreased blade thickness affects the propeller performance.

Program verification

Table 2 shows geometrical data for the MAU 3-60 model propeller.[19] The model propeller is operated at a depth of 25 cm, an advance speed of 0 ~ 2.04 m/s, and a rotation of 12 rpm. The Reynolds number for a radius ratio 0.7 ranged from 4.78×10^5 to 5.11×10^5. The experimental results[20] used a dummy hub method to modify the friction force. We applied Eq. 8 to generate the structural mesh and the mesh for the fluid analysis ignoring the distribution of blade thickness. The structural mesh was 12×12 and the fluid mesh was 8×8 for each blade. Figures 5–7 show the thrust coefficient K_T $(=T/\rho n^2 D^4)$, the torque coefficient K_Q $(=Q/\rho n^2 D^5)$, and efficiency η_0 $(=TV_a/2n\pi Q)$ (T is the thrust force, Q the torque moment, V_a the advance velocity of the ship, D the diameter of the propeller, and n the rotation speed of propeller). The general agreement between the present approach, the Propeller Steady Flow program (PSF2), and experiments leads to the conclusion that the present nonlinear approach is satisfactory for calculating the performance of a propeller blade. The hydroelastic calculation can be

Table 2. Characteristics of MAU 3–60 propeller

r/R	C/D	P/D	Skew	Rake/D	t/D	f/D
0.2	0.3108	0.77	−9.00	0.0176	0.0430	0.1385
0.3	0.3629	0.77	−7.40	0.0265	0.0383	0.1055
0.4	0.4067	0.77	−5.50	0.0353	0.0335	0.0824
0.5	0.4406	0.77	−3.50	0.0441	0.0288	0.0653
0.6	0.4629	0.77	−1.30	0.0529	0.0240	0.0519
0.7	0.4654	0.77	1.08	0.0617	0.0193	0.0414
0.8	0.4340	0.77	3.75	0.0705	0.0146	0.0337
0.9	0.3439	0.77	6.68	0.0794	0.0098	0.0284
0.95	0.2597	0.77	7.76	0.0838	0.0074	0.0284
1.0	0.0000	0.77	9.10	0.0882	0.0000	0.0000

Number of blades, 3; expanded area ratio, 0.6; design advance coefficient, 0.5.

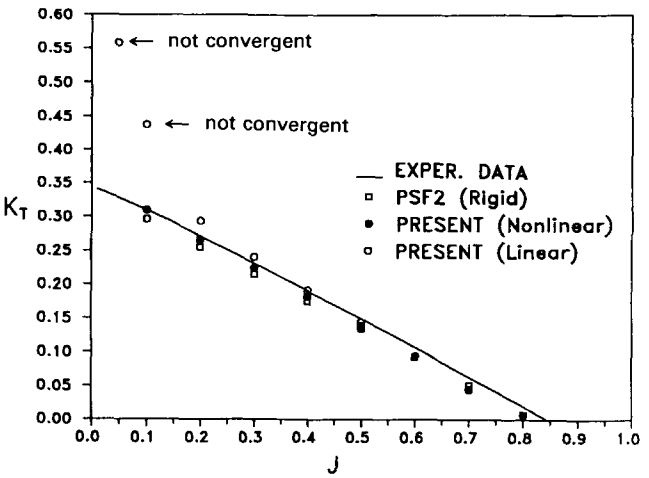

Fig. 5. The thrust coefficient characteristics of the MAU 3-60 propeller

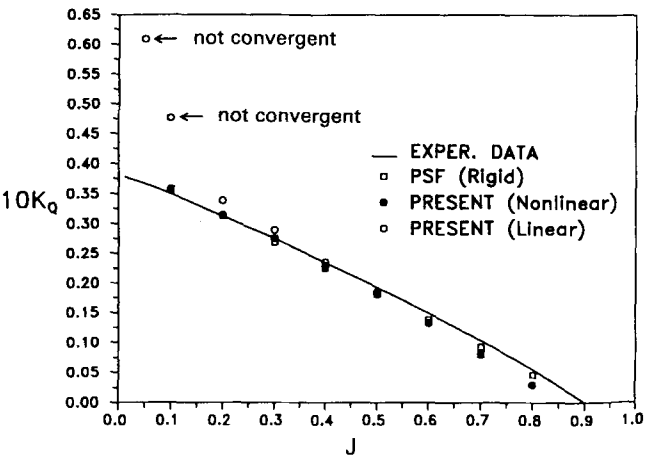

Fig. 6. The torque coefficient characteristics of the MAU 3-60 propeller

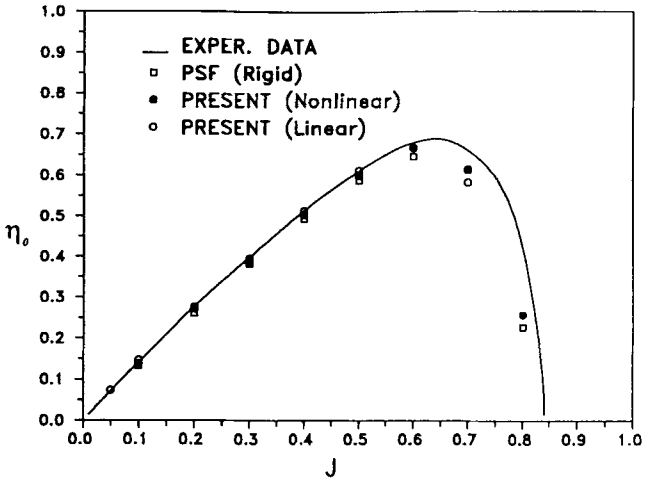

Fig. 7. Efficiency characteristics of the MAU 3-60 propeller. *PSF*, propeller steady flow

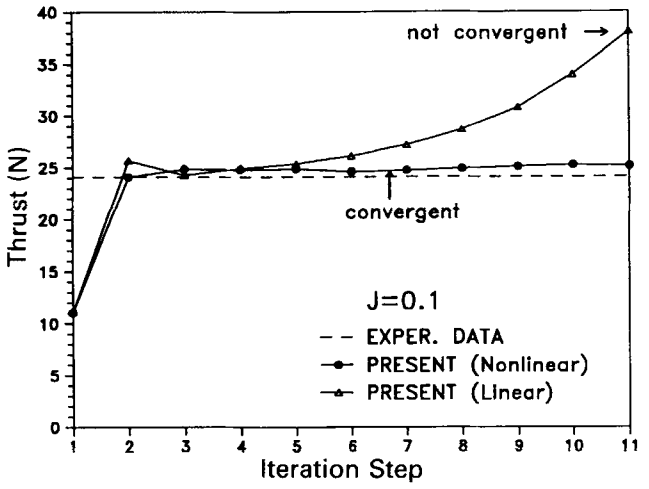

Fig. 8. Thrust loading variation

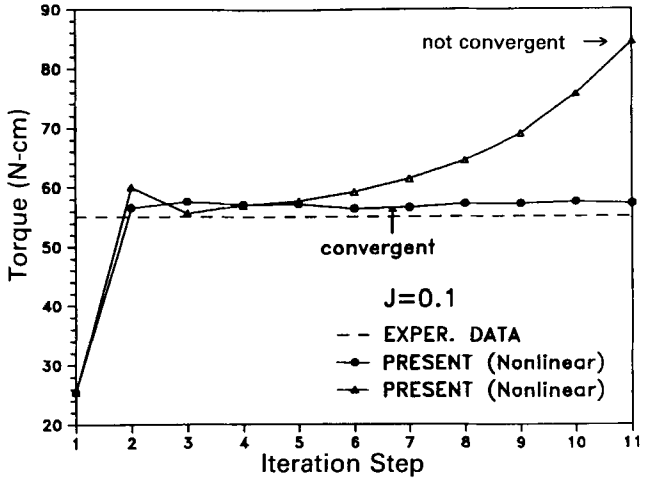

Fig. 9. Torque variation

improved according to the numerical results calculated by PSF2 at small advance coefficients, J. In the PSF2 program it is assumed that the propeller is rigid for the calculation of the performance of the propeller. The linear approach overestimates the response of the blade as well as the thrust and torque forces for small advance coefficients. In the design region the differences between PSF2, the nonlinear approach, and the linear approach are small. The three approaches generate the same result for the efficiency coefficient. The thrust force and torque moment of each iterative calculation for $J = 0.1$ are shown in Figs. 8, 9. The thrust and torque of the nonlinear approach gradually approaches the experimental data but those from the linear approach do not. The pitch distortion of each iterative calculation is shown in Fig. 10. The undeflected pitch is corrected for the viscous effect. The pitch variation of the nonlinear approach is smaller than that of the linear approach. The radial distribution of the camber distortion in the nonlinear approach for $J = 0.1$ is shown in Fig. 11. The camber of the blade does not vary in the blade root region and its maximum variation occurs at about 70% of the radius. The maximal chordwise variation is approximately located at the midchord of each section. The effect of camber distortion increases the thrust force of the blade. The deformed shape of the propeller according to the nonlinear approach is shown in Fig. 12. The maximum deformation is reached at the blade tip.

Effect of blade thickness

The thickness of the blade directly affects the strength of the blade. We decreased the blade thickness and examined the effect on performance and strength of the propeller. A decreased thickness of the blade implies that the stiffness of the blade is likewise decreased, so

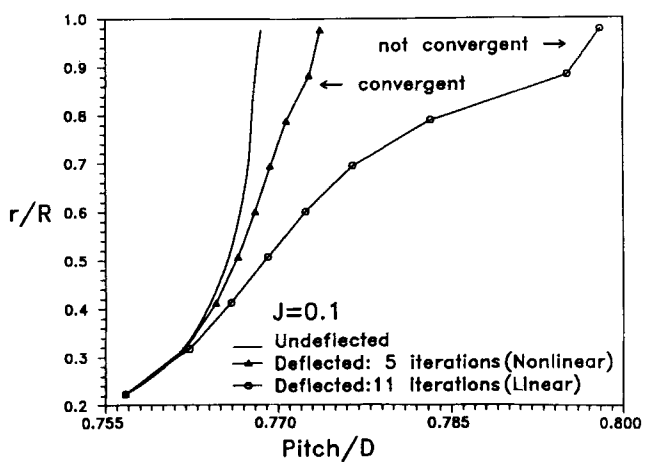

Fig. 10. Pitch variation

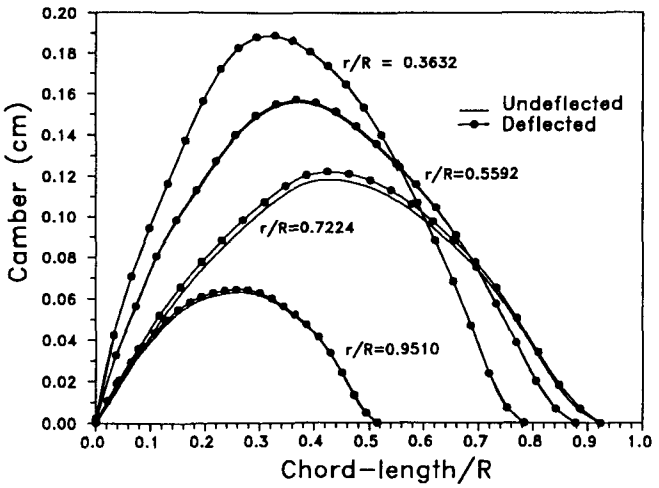

Fig. 11. Camber distribution

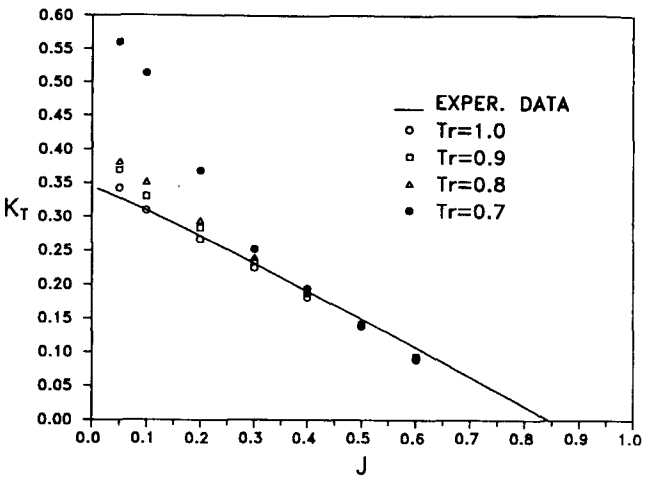

Fig. 13. The thrust coefficient as a function of Tr

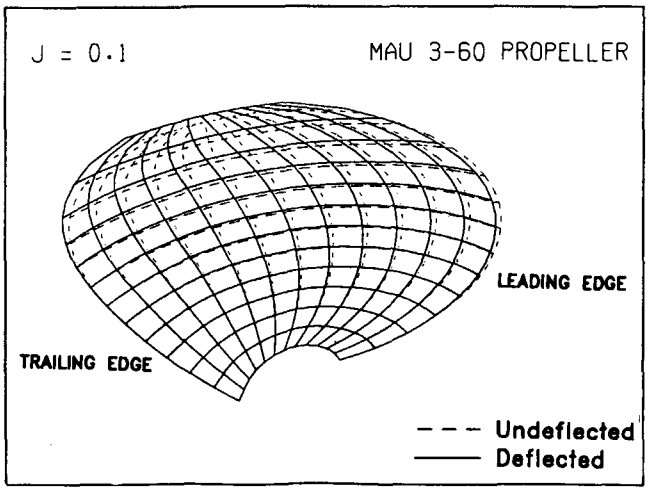

Fig. 12. Deformed propeller shape

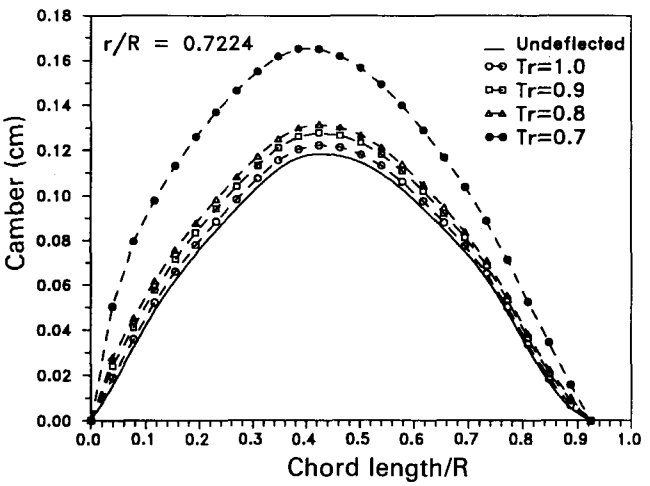

Fig. 14. Camber distortion as a function of Tr

that the blades are more easily deflected. The stress fields of the blade are calculated and justified according to the Tresca yield criteria. We define a thickness reduction factor Tr as the ratio of a given thickness to the original thickness of the blade. The propeller is operated under the same conditions as mentioned above. Figure 13 shows that the thrust coefficient K_T varies with advance coefficient J, and K_T increases with decreased blade thickness for small values of the advance coefficient. K_T does not vary with Tr at a large advance coefficient J. K_T increases rapidly when Tr equals 0.7 because the camber and pitch also increase rapidly (Figs. 14 and 15). The changes in torque coefficient K_Q with J (Fig. 16) are the same as for the thrust coefficient K_T. Figure 17 shows that a decreased blade thickness does not affect the efficiency of the propeller.

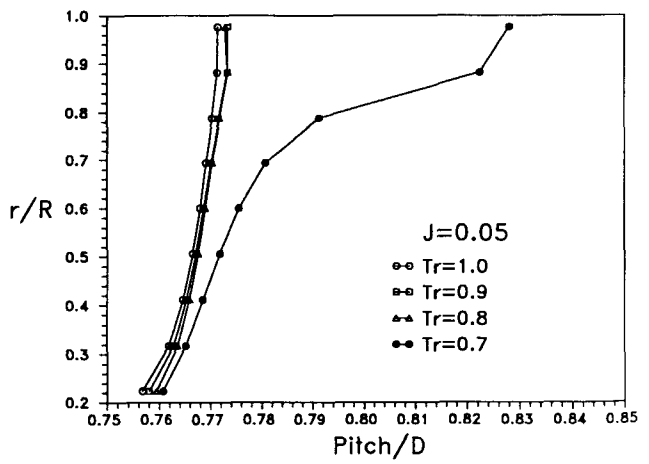

Fig. 15. Pitch distortion as a function of Tr

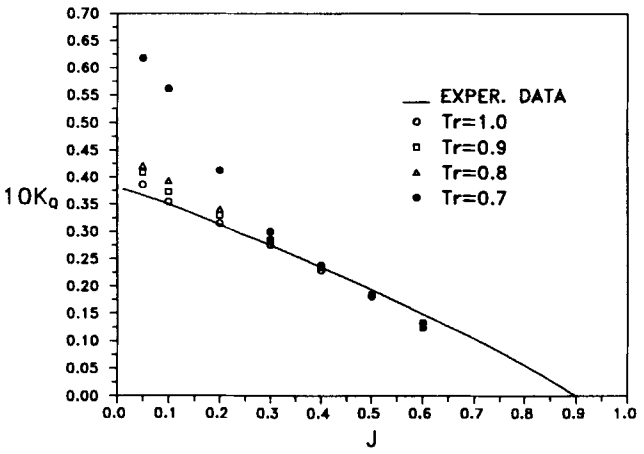

Fig. 16. The torque coefficient as a function of Tr

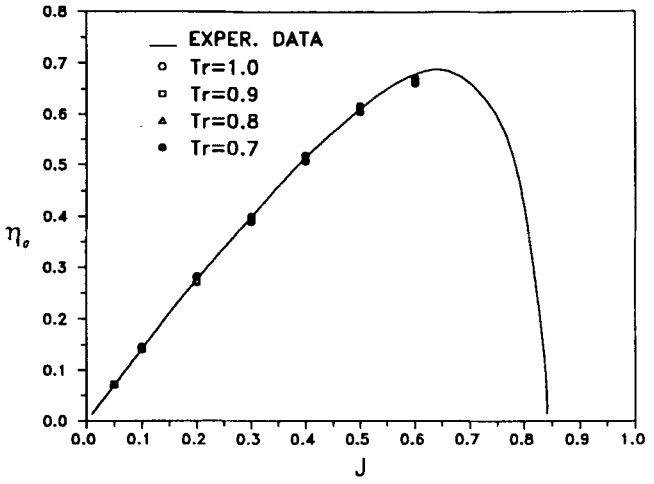

Fig. 17. Efficiency as a function of Tr

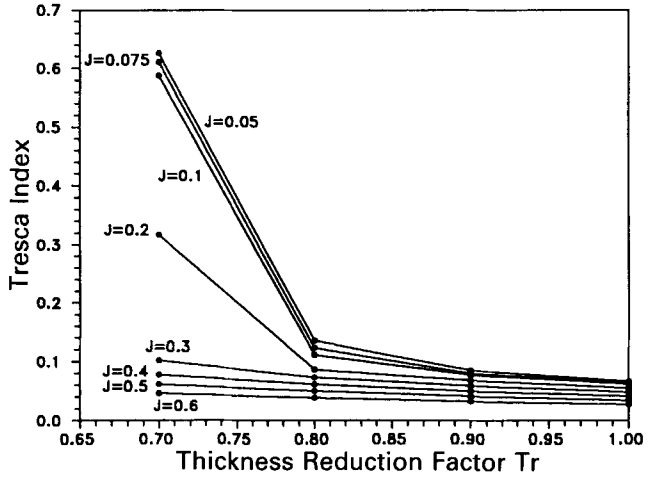

Fig. 18. Value of the Tresca index

The safety factor is set to 2 to calculate the strength of the propeller. The Tresca index for various Tr values is shown in Fig. 18. The value of the Tresca index is less than 0.2 for Tr between 1.0 and 0.8. Hence if we choose Tr to be 0.8, we can save one fifth the weight of the propeller and its strength still suffices. When Tr equals 0.7 and the advance coefficient J is less than 0.2, the Tresca index increases rapidly; its maximal value is about 0.64.

Conclusions

We used a geometrically nonlinear finite-element procedure in conjunction with a noncavitating PSF2 lifting surface analysis to derive a coupled formulation of the fluid and structure and investigated in an iterative manner the hydroelastic effects on a marine propeller. We showed a favorable comparison between calculated values for thrust K_T, torque K_Q, and efficiency η_0 and the data from a steady open water experiment with a MAU 3-60 propeller. Computed and measured values of K_T, K_Q, and η_0 agree satisfactorily except for the numerical results of the linear uncoupled approach at small advance coefficients.

Hydroelastic effects have been shown to influence the performance of propellers and their inclusion in the analysis can improve the numerical results. The strength of the propeller was examined by decreasing the thickness of the blade in the nonlinear model and applying the Tresca yield criterion. In this case, a decreased blade thickness increased propeller deflection, thrust, and torque but did not alter the efficiency of the propeller.

Acknowledgments. This work was supported by the National Science Council of the Republic of China, under the Grant No. NSC 83-0209-E-002-019.

References

1. Taylor DW (1993) The speed and power of ships. Ransdell, Washington
2. Cohen JW (1955) On stress calculations in helicoidal shells and propeller blades. Netherlands Research Center T.N.O. shipbuilding and Navigation, Delft Report 21S
3. Conolly JE (1974) Strength of propellers. Trans RINA 103: 139–204
4. Genalis P (1970) Elastic strength of propellers—an analysis by matrix methods. Ph.D. dissertation. University of Michigan
5. Atkinson P (1968) On the choice of method for the calculation of stress in marine propellers. Trans RINA 110:447–463
6. Ma JH (1974) Stresses in marine propellers. J Ship Res 18: 252–264
7. Sontvedt T (1974) Propeller blade stresses—application of finite-element methods. Comput Struct 4:193–204
8. Atkinson P, Glover EJ (1988) Propeller hydroelastic effects. SNAME on the propeller. '88 Symposium No. 21, Jersey, NJ

9. Szantyr JA (1985) A new method for the analysis of propeller cavitation and hull surface pressures. Trans RINA 127:153–167
10. Zienkiewicz OC (1991) The finite-element method, 4th edn. McGraw-Hill, London
11. Bathe KJ, Bolourchi S (1980) A geometrical and material nonlinear plate and shell element. Comput Struct 11:23–48
12. Haisler WE, Stricklin JA (1972) Development and evaluation of solution procedures for geometrically nonlinear structural analysis. J. American Institute of Aeronautics and Astronautics 10:264–272
13. Bathe KJ, Ramm E (1975) Finite-element formulations for large deformation dynamic analysis. Int J Numer Methods Eng 9: 353–386
14. Chang TY, Sawamiphakdi K (1981) Large deformation analysis of laminated shell by the finite-element method. Comput Struct 13:331–340
15. Sreenivasamurthy S, Ramamurti V (1981) A parametric study of vibration of rotating pre-twisted and tapered low aspect ratio cantilever plates. J Sound Vib 76:311–328
16. Leissa AW, Lee JK, Wang AJ (1982) Rotating blade vibration analysis using shells. ASME J Eng Power 104:296–302
17. Kerwin JE, Lee CS (1978) Prediction of steady and unsteady marine propeller performance by numerical lifting-surface theory. Trans SNAME 86:218–253
18. Singh RK, Kant T, Kakodkar A (1991) Coupled shell-fluid interaction problems with degenerate shell and three-dimensional fluid elements. Comput Struct 38:515–528
19. Yokoo K, Yazaki T (1973) The design method and chart of the propellers of small ships (in Japanese). Seizando, Tokyo
20. Chen CS, Wu TU, Chiou YY (1993) Study on the propulsion performance of an improved FRP inshore fishing boat. Master's thesis, National Taiwan University